International Journal of Rock Mechanics & Mining Sciences 56 (2012) 146–160

Contents lists available at SciVerse ScienceDirect

International Journal of Rock Mechanics & Mining Sciences

journal homepage: www.elsevier.com/locate/ijrmms

Failure criteria for rocks based on smooth approximations to Mohr–Coulomb and Hoek–Brown failure functions

Youn-Kyou Lee [a], S. Pietruszczak [b], Byung-Hee Choi [c,*]

[a] Department of Coastal Construction Engineering, Kunsan National University, Miryong-Dong, Gunsan, Jeonbuk 573–701, South Korea
[b] Department of Civil Engineering, McMaster University, 1280 Main Street West, Hamilton, ON, Canada L8S 4L7
[c] Korea Institute of Geoscience and Mineral Resources, Gwahang-no 92, Yuseong-gu, Daejeon 305–350, South Korea

ARTICLE INFO

Article history:
Received 16 August 2011
Received in revised form
22 May 2012
Accepted 27 July 2012
Available online 29 August 2012

Keywords:
Rock strength
Failure criteria
Intermediate principal stress
Mohr–Coulomb criterion
Hoek–Brown criterion
Anisotropy

ABSTRACT

Existing experimental evidence from true triaxial test (also referred to as poly-axial test) indicates that the influence of the intermediate principal stress (σ_2) on rock strength is substantial. In order to consider this effect in rock engineering design, an adequate 3D failure criterion, which takes into account the effect of σ_2, is required. Such a criterion should not only be a convex but also a smooth function of stress state; the latter to avoid singularities and to ensure the numerical stability. The most popular failure criteria used in rock mechanics, i.e., Mohr–Coulomb (M–C) and Hoek–Brown (H–B), both ignore the effect of σ_2 and also have singular corners. Hence, in this paper, the M–C and H–B criteria are modified to their 3D versions based on geometric approximations of deviatoric sections that lead to smooth and convex surfaces for a wide range of strength parameters. The derived criteria inherit all the key properties of the original ones and are formulated in terms of stress invariants introduced by Nayak and Zienkiewicz. The latter provides an easy way to identify the strength parameters from non-linear multiple regression analysis using the poly-axial test data. In order to validate the proposed criteria, eight sets of poly-axial tests selected from literature are fitted. The results clearly show that the new criteria are quite accurate for all rock types considered. Finally, an extension of the proposed criteria to account for anisotropic rock conditions is discussed and an illustrative example is provided incorporating the functional forms of H–B and modified H–B criteria.

1. Introduction

In rock engineering practice, the conditions at failure are often described by the linear Mohr–Coulomb (M–C) or the non-linear Hoek–Brown (H–B) criterion, which is largely due to their simplicity in formulation and the large amount of experimental data available. Both these criteria are expressed in terms of the major (σ_1) and the minor (σ_3) principal stresses and, as such, are classified as 2D. For intact rock, M–C and H–B criteria are defined in terms of two independent parameters; the internal friction angle (ϕ) and the uniaxial compressive strength (σ_c) (equivalently, the cohesion c) for M–C, and m together with σ_c for H–B criterion. Both criteria mentioned above suffer from limitations arising from ignoring the effect of the intermediate principal stress (σ_2) on rock strength. Moreover, there are significant difficulties in their numerical implementation as their gradient functions become singular in triaxial compression ($\sigma_1 > \sigma_2 = \sigma_3$) and triaxial extension ($\sigma_1 = \sigma_2 > \sigma_3$) regimes.

Much of the experimental evidence accumulated so far [1–5] strongly suggests that σ_2 has a considerable effect on rock strength. To incorporate the influence of σ_2, several general failure criteria have been proposed, among which Drucker–Prager [6], Modified Lade [7], Modified Wiebols and Cook [8], Mogi–Coulomb [9], 3D Hoek–Brown [10], the so-called HBMN [11] and the Unified Strength [12] criteria are well-known. The first four of them are defined by the M–C constants, ϕ and c, while the 3D Hoek–Brown and the HBMN criteria incorporate the H–B constants, m and σ_c. According to several comparative studies [13–16], none of the existing 3D failure criterion has a significant advantage over the others, from both mathematical and practical point of view. For instance, among the 3D criteria mentioned above, only three criteria, i.e., Drucker–Prager, Modified Lade and HBMN, meet the requirements of smoothness and convexity simultaneously. However, the strength prediction by Drucker–Prager is not consistent with the experimental evidence as it yields an identical value for both the triaxial compression and extension regimes. Moreover, the Modified Lade's criterion predicts different strength than M–C criterion for the conditions of triaxial extension.

Identification of strength parameters from the poly-axial test data is another challenge in the course of development of 3D

* Corresponding author. Tel.: +82 42 868 3237; fax: +82 42 868 3416.
E-mail address: bhchoi@kigam.re.kr (B.-H. Choi).

1365-1609/$ - see front matter © 2012 Elsevier Ltd. All rights reserved.
http://dx.doi.org/10.1016/j.ijrmms.2012.07.032

failure criteria. Even for 2D criteria, such as M–C and H–B, identifying the strength parameters which best-fit the whole series of poly-axial data is very difficult. Recently, Colmenares and Zoback [14] and Benz and Schwab [13] employed the grid search method to select the best-fit parameters. This approach, however, turned out to be inaccurate as discussed later in Section 5 of this paper. In the last decade, with the advent of various new 3D failure criteria, the effect of σ_2 has been more frequently considered in solving practical rock mechanics problems such as the borehole stability analysis [16,17], the estimation of ultimate bearing capacity of rock foundation [18] and the analysis of fault slip behavior [19].

In this paper, both M–C and H–B criteria are extended based on the geometrical approximation of their deviatoric shapes that satisfy both the convexity and the smoothness requirements for the practical range of the strength parameters. For convenience of formulation, these failure criteria are expressed in terms stress invariants introduced by Nayak and Zienkiewicz [20]. Non-linear multiple regression technique is introduced to select the related best-fitting parameters by considering the whole series of poly-axial test data together. The performance of the proposed criteria is validated by demonstrating the accuracy in reproducing eight sets of poly-axial test selected from the literature. Finally, an extension of the proposed criteria to account for anisotropy of microstructure is briefly discussed and an illustrative example is provided examining the directional sensitivity of strength.

2. Geometric representation of failure criteria

2.1. Stress state in terms of stress invariants

The stress state σ_{ij} can be conveniently represented as a point $P(\sigma_1,\sigma_2,\sigma_3)$ in the principal stress space, as shown in Fig. 1. The plane passing through P and perpendicular to the hydrostatic axis is referred to as the deviatoric (or octahedral) plane and ξ is the distance from the origin at O. In the deviatoric plane itself, ρ is the radial distance defining the location of P; while θ, known as the Lode's angle, is the measure of rotation from σ_1^* -axis, which is the projection of σ_1-axis on the deviatoric plane. For $\sigma_1 \geq \sigma_2 \geq \sigma_3$, the angle θ varies within the range $0 \leq \theta \leq \pi/3$.

The set of parameters ξ, ρ, and θ provides a convenient alternative to the basic invariants for the representation of the failure criteria. According to Nayak and Zienkiewicz [20], these invariants are related to the basic invariants as

$$\xi = \frac{I_1}{\sqrt{3}}, \quad \rho = \sqrt{2J_2}, \quad \theta = \frac{1}{3}\cos^{-1}\left(\frac{3\sqrt{3}}{2}\frac{J_3}{J_2^{3/2}}\right) \tag{1}$$

where $I_1=\sigma_{ii}$ is the first invariant of the stress tensor σ_{ij}, while $J_2=s_{ij}s_{ij}/2$ and $J_3=s_{ij}s_{jk}s_{ki}/3$ are the second and third invariants of the stress deviator $s_{ij}=(\sigma_{ij}-\sigma_{kk}\delta_{ij}/3)$. Then, the three principal stresses $\sigma_1 \geq \sigma_2 \geq \sigma_3$ can be expressed in terms of ξ, ρ, and θ as

$$\begin{Bmatrix}\sigma_1\\ \sigma_2\\ \sigma_3\end{Bmatrix} = \sqrt{\frac{2}{3}}\rho\begin{Bmatrix}\cos(\theta)\\ \cos(\theta-\frac{2\pi}{3})\\ \cos(\theta+\frac{2\pi}{3})\end{Bmatrix} + \frac{\xi}{\sqrt{3}} \tag{2}$$

2.2. General types of failure criteria for rock

The condition at failure in a rock can be described by the general form

$$F(\xi,\rho,\theta)=0 \tag{3}$$

which allows for a very straightforward geometrical interpretation. Assuming a constant value of θ in Eq. (3) gives a meridian section relating ξ and ρ at failure, whereas substitution of $\xi=const.$ yields the locus of the failure surface in the deviatoric plane.

The linear form of Eq. (3) can be expressed as

$$F_L = \rho - g_L(\theta)(\alpha\xi+\beta)=0 \tag{4}$$

where α, β are material constants and $g_L(\theta)$ is the function satisfying the condition

$$g_L(0)=1; \quad g_L\left(\frac{\pi}{3}\right)=\frac{\rho|_{\theta=\pi/3}}{\rho|_{\theta=0}}=k \tag{5}$$

in which $\rho|_{\theta=0}$ is the value of ρ at failure for the triaxial compression regime ($\sigma_1 \geq \sigma_2=\sigma_3$), while $\rho|_{\theta=\pi/3}$ denotes the value of ρ at failure for the triaxial extension ($\sigma_1=\sigma_2 \geq \sigma_3$). The function $g_L(\theta)$ in Eq. (4), which is independent of ξ here, defines the shape of the deviatoric cross-section of the failure criterion.

On the other hand, the non-linear versions of Eq. (3) for geomaterials are generally of the type

$$F_{NL} = \rho - g_{NL}(\theta,\xi)\rho_c = 0 \tag{6}$$

where g_{NL}, which again defines the shape of the deviatoric cross-section, now depends not only on θ but also on ξ. Furthermore,

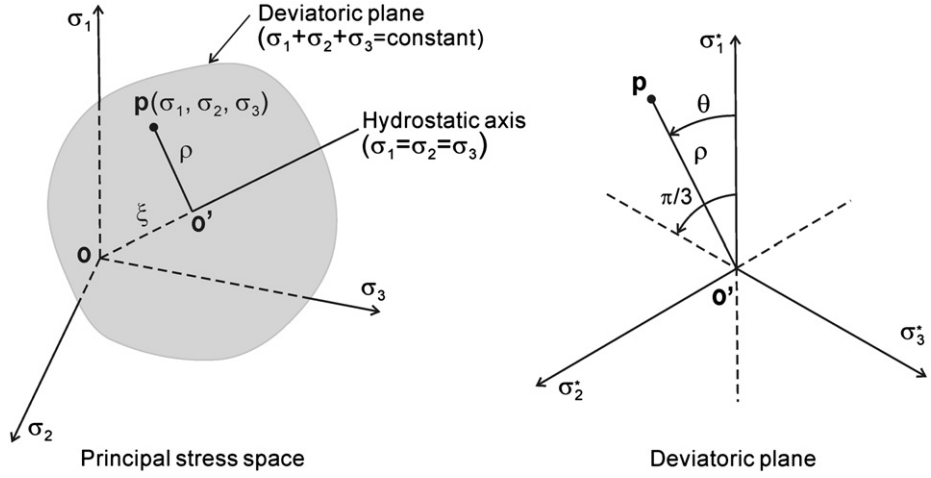

Fig. 1. A stress state in the principal stress space and in the deviatoric plane.

g_{NL} satisfies the conditions

$$g_{NL}(0,\xi)=1; \quad g_{NL}\left(\frac{\pi}{3},\xi\right)=k(\xi) \tag{7}$$

It should be noted that ρ_c in Eq. (6), which represents the maximum value of ρ in the triaxial compression domain ($\theta=0$), i.e., $\rho_c=\rho|_{\theta=0}$, is a non-linear function of ξ. All the deviatoric cross-sections corresponding to representation (6) are geometrically similar if $k(\xi)=const.$, whereas the sections evolve if $k(\xi)$ varies along the hydrostatic axis.

In Eqs. (5) and (7), k is physically admissible if it is in the range of $0.5\le k\le 1$. Moreover Drucker's stability postulate [21] requires that the failure surfaces, $F_L=0$ and $F_{NL}=0$, be convex, so that g_L and g_{NL} should be convex in the entire range of $0\le\theta\le\pi/3$ and at the same time ρ_c of Eq. (6) should be a convex function of ξ.

3. Approximation to the M–C criterion

3.1. The basic M–C function

In spite of obvious limitations arising from neglecting the effect of the intermediate principal stress, the M–C condition at failure is the most common linear criterion employed for geomaterials. This criterion postulates that the failure within the rock occurs when σ_1 and σ_3 satisfy the condition

$$\sigma_1=\left(\frac{1-\sin\phi}{1+\sin\phi}\right)\sigma_3+\frac{2c\cos\phi}{1-\sin\phi} \tag{8}$$

where ϕ and c are the internal friction angle and the cohesion, respectively. Combining Eq. (8) with Eq. (2) yields the failure function in terms of ξ, ρ, and θ as

$$F_{MC}=\rho-g_{MC}(\theta)(\alpha_{MC}\xi+\beta_{MC})=0 \tag{9}$$

where

$$g_{MC}(\theta)=\frac{3-\sin\phi}{\cos\theta(3-\sin\phi)+\sqrt{3}\sin\theta(1+\sin\phi)}; \quad \alpha_{MC}=\frac{2\sqrt{2}\sin\phi}{3-\sin\phi}; \quad \beta_{MC}=\frac{2\sqrt{6}c\cos\phi}{3-\sin\phi} \tag{10}$$

It should be noted that $g_{MC}(\theta)$ satisfies

$$g_{MC}(0)=1; \quad g_{MC}\left(\frac{\pi}{3}\right)=\frac{3-\sin\phi}{3+\sin\phi} \tag{11}$$

Due to permuting nature of the principal axes, Eq. (9) represents the six-fold irregular hexagonal pyramid in the principal stress space. As shown in Fig. 2 (here $\rho_c=\rho|_{\theta=0}$ and $\rho_t=\rho|_{\theta=\pi/3}$), the cross-sectional shape in the deviatoric plane is an irregular hexagon (independent of ξ), while the meridians are straight lines. The existence of corners, where the gradient is not uniquely defined, apparently poses difficulties in the numerical implementation.

3.2. Three dimensional approximation to M–C criterion

Various approximations to M–C criterion can be obtained by replacing $g_{MC}(\theta)$ in Eq. (9) by a suitable function $g_L(\theta)$ satisfying the constraint (5) with $k=(3-\sin\phi)/(3+\sin\phi)$. It is desirable that $g_L(\theta)$ be not only continuous but also a convex function within the range $0\le\theta\le\pi/3$, satisfying

$$\frac{dg_L(\theta)}{d\theta}=0 \quad \text{at } \theta=0,\frac{\pi}{3} \tag{12}$$

to guarantee the non-singularity.

Jiang and Pietruszczak [22] provided an extensive discussion on the convexity of frequently used forms of $g_L(\theta)$'s in plasticity together with their own one. Among them, the expression proposed by Willam and Warnke [23] is quite attractive since it is unconditionally convex and smooth for the entire range $0.5\le k\le 1$ due to its elliptical nature. This expression takes the form

$$g_{WW}(\theta)=\frac{2(1-k^2)\cos(\theta-(\pi/3))+(2k-1)\sqrt{4(1-k^2)\cos^2(\theta-(\pi/3))+5k^2-4k}}{4(1-k^2)\cos^2(\theta-(\pi/3))+(2k-1)^2} \tag{13}$$

Despite of its mathematical robustness, Eq. (13) is quite complex. A somewhat simpler expression, which also ensures convexity in a broad range of k values, was proposed by Jiang and Pietruszczak [22] as

$$g_{JP}(\theta)=\frac{\left(\sqrt{1+f}-\sqrt{1-f}\right)k}{k\sqrt{1+f}-\sqrt{1-f}+(1-k)\sqrt{1-f\cos 3\theta}} \tag{14}$$

where $f\to 1$ is a constant. It should be noted that, for $f=1$, Eq. (14) is singular at $\theta=0$, whereas $f\to 1$ yields a smooth locus in the deviatoric plane. Setting $f=0.999$, for example, Eq. (14) is convex in the range $0.56\le k\le 1$, which corresponds to $0\le\phi\le 57.8^\circ$. For most rocks, the internal friction angles are within this range. Eqs. (13) and (14) yield circular cross-sections when $k=1$, while the cross-sections become curvilinear triangles as $k\to 0.5$.

In this paper, representation (14) is adopted with $f=0.999$ as a replacement of $g_{MC}(\theta)$ to extend the M–C criterion to its three dimensional version, which depends on the intermediate principal stress. Thus, the approximation to M–C surface, referred

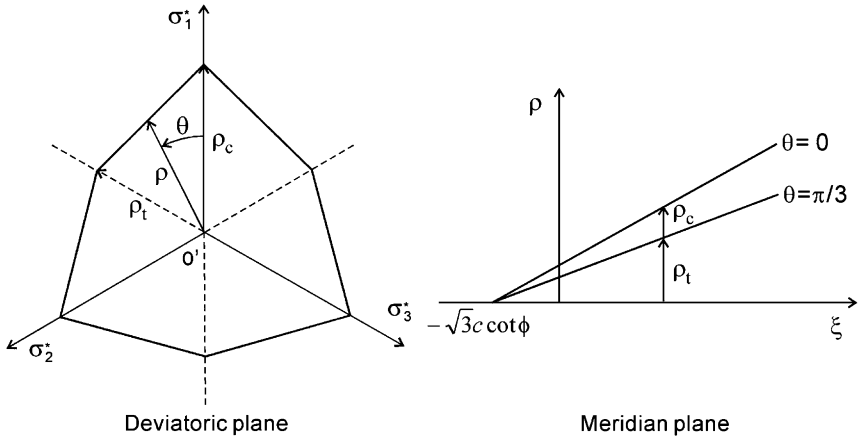

Fig. 2. M–C criterion in the deviatoric and the meridian planes.

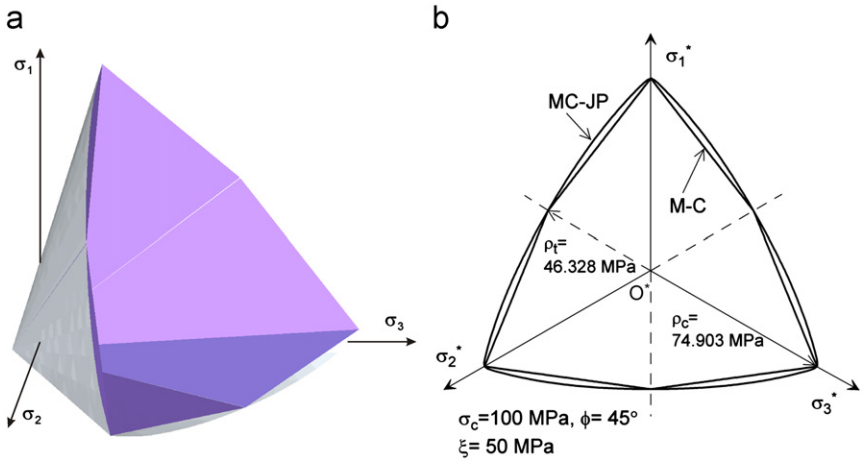

Fig. 3. The MC–JP and the M–C failure criteria (a) in the principal stress space and (b) in the deviatoric plane.

to as the MC–JP hereafter, takes the form

$$F_{MC-JP}=\rho-g_{JP}(\theta)(\alpha_{MC}\xi+\beta_{MC})=0 \tag{15}$$

Apparently, for $k=1$, Eq. (15) reduces to the Drucker–Prager criterion [6].

As an illustrative example, Fig. 3 shows the MC–JP surface together with the corresponding M–C surface, for the rock sample having the strength parameters of $\sigma_c=100$ MPa and $\phi=45^\circ$. The deviatoric cross-sections correspond to $\xi=50$ MPa. Here, σ_c is related to cohesion (c) and the internal friction angle (ϕ) by $\sigma_c=2c\cos\phi/(1-\sin\phi)$. The figure clearly shows that the MC–JP surface is smooth and convex, while it passes through the corners of the M–C hexagon; this feature offers a great advantage in numerical application over the criteria having singular corners.

The influence of the intermediate principal stress on rock strength is examined in Fig. 4, which shows the results for MC–JP criterion for a rock sample with $\sigma_c=50$ MPa and $\phi=38^\circ$. The predictions are compared with those corresponding to M–C criterion as well as Modified Wiebols and Cook criterion [8,14]. As the original M–C criterion does not take into account the effect of σ_2, the results are depicted as horizontal lines. The Modified Wiebols and Cook criterion does depend on σ_2, but it can be shown that the gradient of the failure function cannot be uniquely defined in triaxial compression regime ($\theta=0$). The strength (σ_1) as predicted by MC–JP criterion is larger than that corresponding to standard M–C form, except for the triaxial compression ($\theta=0$) and triaxial extension ($\theta=\pi/3$) regimes, where the predictions are identical, as the two envelopes match each other along the corresponding meridians.

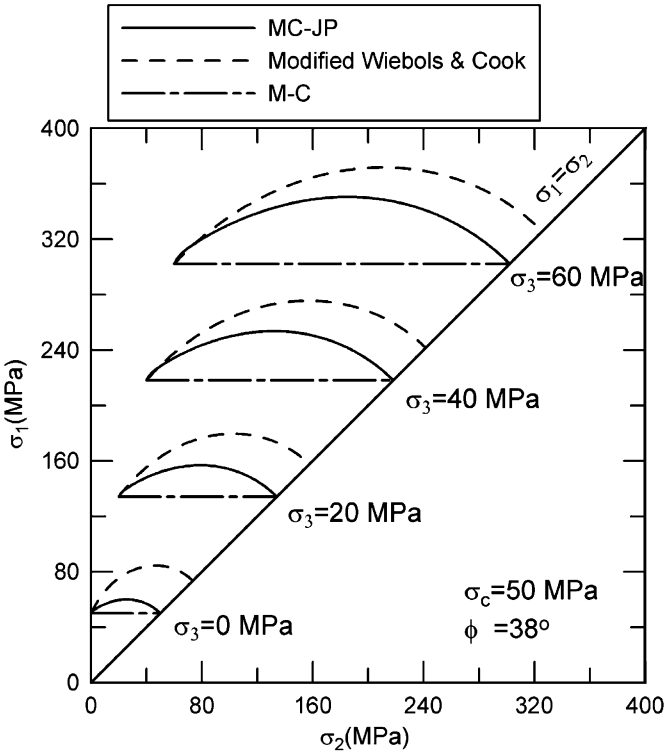

Fig. 4. Sensitivity of the triaxial strength (σ_1) to the intermediate stress (σ_2) in the MC–JP and Modified Wiebols and Cook criteria.

4. Approximation to H–B criterion

4.1. The basic H–B function

The empirical equation proposed by Hoek and Brown [24] assumes that rock fails if the major and minor principal stresses satisfy the non-linear relation

$$\sigma_1=\sigma_3+\sqrt{m\sigma_c\sigma_3+s\sigma_c^2} \tag{16}$$

where m and s are constants that depend on the characteristics of the rock; s varies within $0\le s\le 1$ and $s=1$ for intact rock material. The H–B criterion has been widely accepted in rock engineering practice since it was derived based on a wide range of experimental data. It is evident that Eq. (16) ignores the influence of the intermediate principal stress σ_2 on the conditions at failure.

Substitution of Eq. (2) into Eq. (16) yields, after some algebraic manipulations, the functional for of H–B criterion in terms of the stress invariants ξ, ρ, and θ, (see Fig. 5)

$$F_{HB}=\rho-\frac{m\sigma_c\cos(\theta+(2\pi/3))+\sqrt{m^2\sigma_c^2\cos^2(\theta+(2\pi/3))+4(\sqrt{3}m\sigma_c\xi+3s\sigma_c^2)\sin^2(\theta+(\pi/3))}}{2\sqrt{6}\sin^2(\theta+(\pi/3))}=0 \tag{17}$$

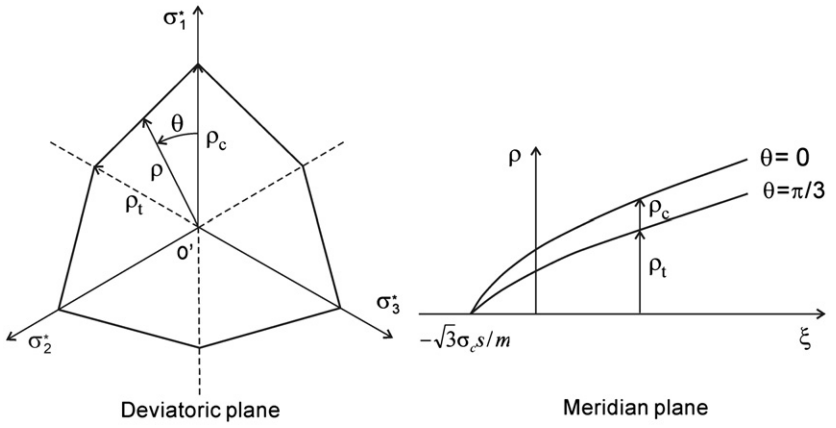

Fig. 5. H–B criterion in the deviatoric and the meridian planes.

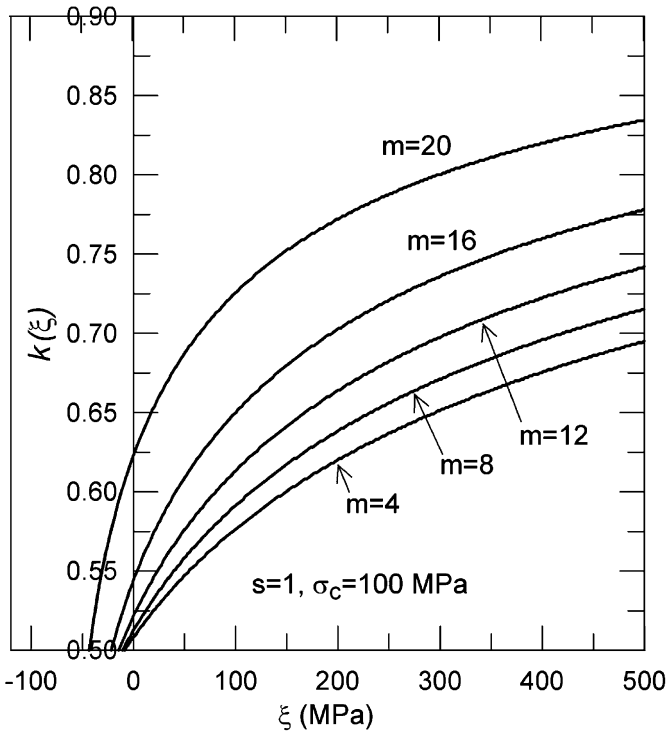

Fig. 6. Variation of k along the hydrostatic axis for different m values.

As in the case of M–C criterion, the H–B criterion is an irregular hexagon in the deviatoric plane, whereas its meridian section is non-linear and has vertex at $\xi=-\sqrt{3}\sigma_c s/m$. According to Eq. (17), ρ_c and ρ_t in Fig. 5 are expressed as

$$\rho_c=\frac{1}{3\sqrt{6}}\left(-m\sigma_c+\sqrt{m^2\sigma_c^2+12\sqrt{3}m\sigma_c\xi+36s\sigma_c^2}\right) \tag{18}$$

$$\rho_t=\frac{2}{3\sqrt{6}}\left(-m\sigma_c+\sqrt{m^2\sigma_c^2+3\sqrt{3}m\sigma_c\xi+9s\sigma_c^2}\right) \tag{19}$$

so that $k(\xi)$ is defined as

$$k(\xi)=\frac{-2m\sigma_c+2\sqrt{m^2\sigma_c^2+3\sqrt{3}m\sigma_c\xi+9s\sigma_c^2}}{-m\sigma_c+\sqrt{m^2\sigma_c^2+12\sqrt{3}m\sigma_c\xi+36s\sigma_c^2}} \tag{20}$$

Fig. 6 shows the plots of Eq. (20), corresponding to $s=1$ and $\sigma_c=100$ MPa, for four different values of parameter m. It can be shown that $k(\xi)\to 0.5$ for $\xi\to-\sqrt{3}\sigma_c s/m$, whereas $k(\xi)\to 1$ for $\xi\to\infty$, which means that the cross-sectional shape of H–B criterion evolves from triangular at low confining pressure to regular hexagonal at very high confining pressure.

4.2. Three dimensional approximation to the H–B criterion

Depending on the choice of the function g_{NL} in Eq. (6), various approximations to H–B criterion may be developed. To maintain the mathematical rigor, g_{NL} should be smooth and convex for all possible values of θ and k. In this paper, the expression by Willam and Warnke's, viz. Eq. (13), is selected as it ensures convexity of the failure loci for all the deviatoric cross-sections. Note that, according to Eq. (20), the Jiang and Pietruszczak's expression, i.e., Eq. (14), violates the requirement of convexity when ξ is small or negative. Substituting Eq. (20) in Eq. (13) and then combining the result with Eqs. (18) and (6), yields the following 3-D version of the H–B surface, referred to thereafter as the HW–WW criterion

$$F_{HB-WW}=\rho-g_{WW}(\theta,\xi)\rho_c=0 \tag{21}$$

Fig. 7 shows the principal stress-space view of the above criterion for a rock with $\sigma_c=100$ MPa, $m=12$ and $s=1$. It is evident that the proposed form circumscribes the H–B surface smoothly, while it coincides with the basic H–B in both the compression and extension regimes. The evolution of the deviatoric cross-sections with ξ is depicted in Fig. 8, which reveals that the degree of asymmetry in the cross-sections diminishes with the increase in the value of ξ.

Fig. 9 demonstrates the effect of the intermediate principal stress σ_2, as predicted by HB–WW criterion, using the same set of material parameters as those in Fig. 7. It is evident that in the general 3-D stress regime, the strength predicted by HB–WW is greater than that predicted by the original H–B form. For example, for $\sigma_3=60$ MPa, the maximum value of σ_1 obtained from HB–WW is 409.33 MPa, which is about 20% higher than that corresponding to the original H–B criterion.

5. Identification of the proposed criteria using the poly-axial test data

5.1. Poly-axial data

In order to validate the performance of the proposed 3-D failure criteria, the poly-axial test (also referred to as true triaxial test) data for eight different rock types have been collected from the literature. The three data sets, i.e., those for Shirahama

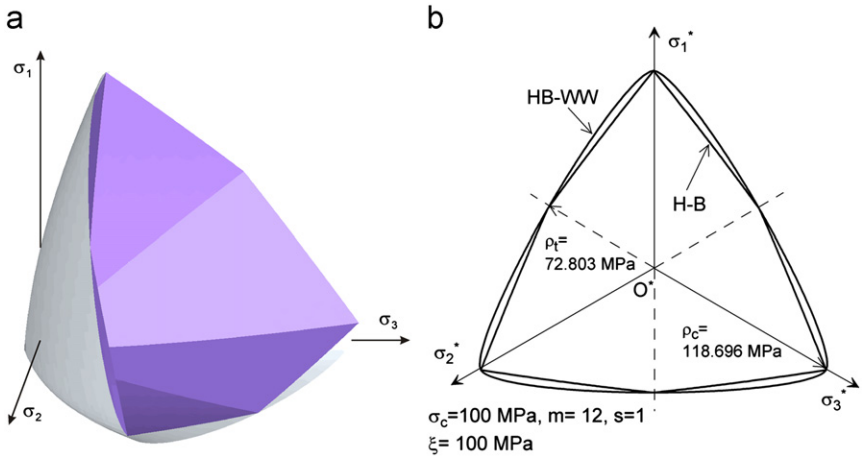

Fig. 7. The HB–WW and H–B failure criteria (a) in the principal stress space and (b) in the deviatoric plane.

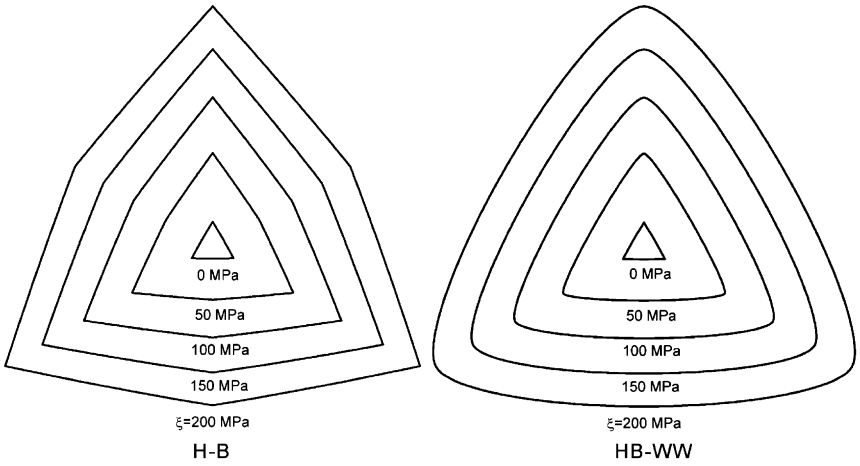

Fig. 8. The evolution of the deviatoric cross-sections in the H–B and HB–WW criteria.

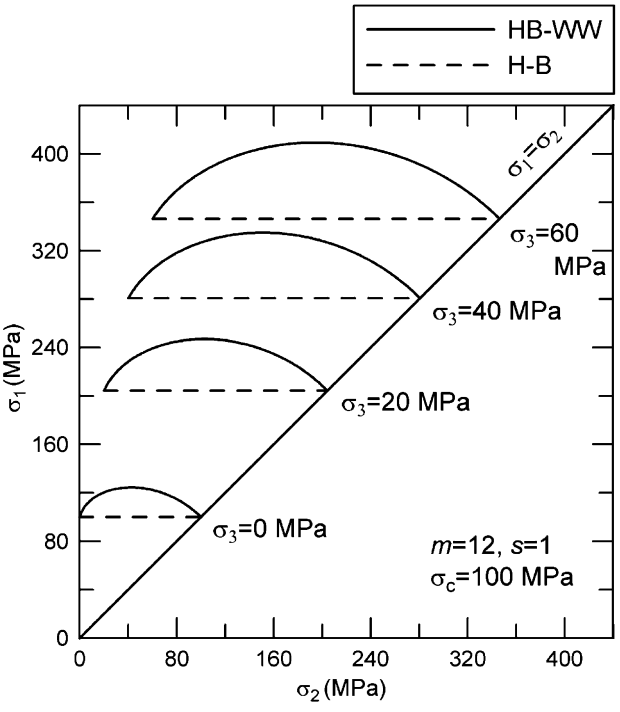

Fig. 9. Sensitivity of the triaxial strength (σ_1) to the intermediate stress (σ_2) in the HB–WW criterion.

sandstone, Yuubari shale and Westerly granite, were obtained from Al-Ajmi and Zimmerman [9]. The first two of them were digitized from the article of Takahashi and Koide [5], while the third was digitized from Haimson and Chang [2]. The other four data sets, i.e., those for Dunham dolomite, Solnhofen limestone, Mizuho trachyte and Manazuru andesite, were taken from Mogi [4]. The remaining one, i.e., that for or KTB amphibolite tested by Chang and Haimson [1], was collected from Colmenares and Zoback [14]. The digital data for these eight sets of poly-axial test data, with the corresponding values of stress invariants at failure, are provided in Tables 1–8.

5.2. Determination of best-fitting strength parameters

One of the convenient features of the proposed 3D failure criteria is that they employ the same strength parameters as the original ones, i.e., ϕ and σ_c (for M–C and the MC–JP) and m, σ_c (for H–B and HB–WW criterion) with the assumption of intact rock, viz. $s=1$. For each data set mentioned in Section 5.1, the best-fitting strength parameters for each criterion were determined and then the strength predictions based on those criteria were compared with the experimental data.

It is worthwhile to note that the value of ρ at failure (viz. Eqs. (9), (15), (17) and (21)), is a non-linear explicit function of ξ and θ. This means that the best-fitting strength parameters could be determined by a non-linear multiple regression analysis on the series of (ξ, ρ, θ) at failure. In this non-linear regression, ρ is considered as a dependent variable, while ξ and θ as two

Table 1
Polyaxial test data for Shirahama sandstone [5,9].

σ_1 (MPa)	σ_2 (MPa)	σ_3 (MPa)	ξ (MPa)	ρ (MPa)	θ (rad)
94	9	5	62.35	71.09	0.04
97	15	5	67.55	71.39	0.10
88	29	5	70.44	60.40	0.28
109	44	5	91.22	74.30	0.38
94	65	5	94.69	64.19	0.72
109	12	8	74.48	80.88	0.03
129	27	8	94.69	92.03	0.15
132	41	8	104.50	90.82	0.26
135	50	8	111.43	91.50	0.33
127	79	8	123.55	84.67	0.63
147	15	15	102.19	107.78	0.00
157	29	15	116.05	110.67	0.09
165	62	15	139.72	108.50	0.31
162	82	15	149.53	104.08	0.47
159	88	15	151.27	101.83	0.53
168	97	15	161.66	108.28	0.57
178	20	20	125.86	129.01	0.00
183	30	20	134.52	129.20	0.05
173	41	20	135.10	117.29	0.13
185	50	20	147.22	124.30	0.17
177	57	20	146.65	116.07	0.23
197	68	20	164.54	129.45	0.27
194	82	20	170.90	124.72	0.36
193	97	20	178.98	122.58	0.46
185	100	20	176.09	116.69	0.51
197	30	30	148.38	136.35	0.00
218	47	30	170.32	147.05	0.08
224	69	30	186.48	145.12	0.19
232	88	30	202.07	147.09	0.28
229	109	30	212.46	141.71	0.41
241	129	30	230.94	149.29	0.49
227	150	30	234.98	140.40	0.65
215	171	30	240.18	136.68	0.82
224	40	40	175.51	150.24	0.00
244	60	40	198.61	159.03	0.09
252	70	40	209.00	162.24	0.13
253	79	40	214.77	160.38	0.17
252	100	40	226.32	154.54	0.28
274	99	40	238.45	172.11	0.24
265	118	40	244.22	161.57	0.35
279	138	40	263.85	169.91	0.42
274	159	40	273.09	165.47	0.53

independent variables. Accordingly, the resulting best-fitting strength parameters could be determined using the least square technique which involves minimizing the object function

$$o = \sum_{i=1}^{n} (\rho_i - \rho_i^*)^2 \tag{22}$$

where n is the number of data point, while ρ_i and ρ_i^* are the experimental and predicted values of ρ, respectively. It should be noted that in this study the best-fitting parameters are calculated from a single round of the regression analysis taking into account all the data points for a specific rock type simultaneously. In this way, the non-linear multiple regression technique provides direct and more rigorous way of finding the best fit parameters than the grid search method [13,14], which requires consideration of a large number of strength parameter combinations in order to construct the misfit contours.

The accuracy of fitting to the actual poly-axial data may be evaluated by use of the residual standard deviation (*RSD*) defined by

$$RSD = \sqrt{\frac{1}{n-2}\sum_{i=1}^{n} (\rho_i - \hat{\rho}_i)^2} \tag{23}$$

where $(n-2)$ specifies the degrees of freedom [25] of the problem and $\hat{\rho}_i$ is the value predicted by the best-fitting model. Apparently, the lower the *RSD* value, the better the match to the experimental data. This kind of non-linear regression can be easily carried out by using standard math software such as Maple.

5.3. Discussion on the results of fitting to the poly-axial data

The non-linear regressions employing the proposed 3D failure criteria, viz. MC–JP and HB–WW, together with their respective original 2D criteria (i.e., M–C and H–B), were carried out to identify the strength parameters. Based on the *RSD* values from the regression analysis, Eq. (23), the ability of the proposed 3D failure criteria to predict the poly-axial strength of rock was assessed. The resulting best-fitting parameters and the corresponding *RSD* values for each rock type are presented in

Table 2
Polyaxial test data for Dunham dolomite [4].

σ_1 (MPa)	σ_2 (MPa)	σ_3 (MPa)	ξ (MPa)	ρ (MPa)	θ (rad)	σ_1 (MPa)	σ_2 (MPa)	σ_3 (MPa)	ξ (MPa)	ρ (MPa)	θ (rad)
400	25	25	259.81	306.19	0.00	682	105	105	515.00	471.12	0.00
475	66	25	326.78	351.88	0.08	778	167	105	606.22	526.02	0.08
495	96	25	355.65	358.30	0.14	786	205	105	632.78	520.04	0.14
560	129	25	412.23	401.17	0.18	805	268	105	680.12	517.99	0.22
571	174	25	444.56	399.13	0.27	863	270	105	714.76	563.75	0.21
586	229	25	484.97	401.57	0.37	824	334	105	729.19	519.46	0.32
545	272	25	486.13	367.85	0.49	840	356	105	751.13	528.36	0.34
487	45	45	333.13	360.89	0.00	822	415	105	774.80	508.54	0.45
570	97	45	411.07	409.09	0.09	725	125	125	562.92	489.90	0.00
576	126	45	431.28	404.57	0.14	824	187	125	655.87	547.18	0.08
606	160	45	468.23	419.07	0.20	860	239	125	706.68	559.42	0.14
639	183	45	500.56	439.63	0.22	863	293	125	739.59	547.04	0.22
670	240	45	551.37	452.24	0.31	897	362	125	799.05	559.28	0.30
670	266	45	566.38	448.21	0.36	941	414	125	854.48	585.12	0.36
622	294	45	554.83	409.27	0.44	918	463	125	869.49	562.77	0.44
568	65	65	402.99	410.70	0.00	886	516	125	881.61	538.18	0.54
638	117	65	473.43	448.13	0.08	883	253	145	739.59	563.68	0.14
644	153	65	497.68	441.24	0.14	927	296	145	789.82	586.65	0.18
687	208	65	554.26	460.71	0.22	923	324	145	803.67	576.23	0.22
685	262	65	584.28	448.01	0.32	922	349	145	817.53	569.70	0.26
746	318	65	651.83	486.81	0.38	1015	392	145	896.05	634.04	0.28
701	393	65	669.15	449.79	0.54	1002	410	145	898.93	620.52	0.31
620	85	85	456.11	436.83	0.00	952	455	145	896.05	575.72	0.39
684	128	85	517.88	472.51	0.06						
719	153	85	552.52	492.25	0.10						
733	233	85	606.80	480.21	0.22						
773	306	85	672.04	496.75	0.32						
818	376	85	738.43	521.96	0.41						
798	445	85	766.72	504.18	0.53						

Table 3
Polyaxial test data for Westerly granite [2,9].

σ_1 (MPa)	σ_2 (MPa)	σ_3 (MPa)	ξ (MPa)	ρ (MPa)	θ (rad)
201	0	0	116.05	164.12	0.00
306	40	0	199.76	235.22	0.12
301	60	0	208.42	225.30	0.19
317	80	0	229.21	233.14	0.25
304	100	0	233.25	219.11	0.33
231	2	2	135.68	186.98	0.00
300	18	2	184.75	237.05	0.05
328	40	2	213.62	252.10	0.11
359	60	2	243.06	270.93	0.15
353	80	2	251.15	260.65	0.21
355	100	2	263.85	257.71	0.27
430	20	20	271.35	334.76	0.00
529	40	20	340.06	407.68	0.03
602	60	20	393.75	459.74	0.06
554	62	20	367.19	419.91	0.07
553	61	20	366.04	419.46	0.07
532	79	20	364.31	396.16	0.11
575	100	20	401.26	424.28	0.13
567	114	20	404.72	413.62	0.16
601	150	20	445.14	431.22	0.21
638	202	20	496.52	449.13	0.29
605	38	38	393.18	462.95	0.00
620	38	38	401.84	475.20	0.00
700	57	38	458.99	532.93	0.03
733	78	38	490.17	551.86	0.05
720	103	38	497.10	532.30	0.09
723	119	38	508.07	529.34	0.11
731	157	38	534.63	524.05	0.16
781	198	38	587.17	553.03	0.21
747	60	60	500.56	560.93	0.00
811	90	60	554.83	601.32	0.04
821	114	60	574.46	600.52	0.06
860	180	60	635.09	610.14	0.14
861	249	60	675.50	592.13	0.23
889	77	77	602.18	663.00	0.00
954	102	77	654.14	706.08	0.03
992	142	77	699.17	722.02	0.06
998	214	77	744.20	702.77	0.14
1005	310	77	803.67	682.76	0.24
1012	100	100	699.75	744.64	0.00
1103	165	100	789.82	793.74	0.06
1147	167	100	816.37	828.87	0.06
1155	216	100	849.28	818.17	0.10
1195	259	100	897.20	836.74	0.13
1129	312	100	889.70	768.39	0.20

Table 4
Polyaxial test data for Yuubari shale [5,9].

σ_1 (MPa)	σ_2 (MPa)	σ_3 (MPa)	ξ (MPa)	ρ (MPa)	θ (rad)
161	25	25	121.82	111.04	0.00
168	25	25	125.86	116.76	0.00
182	35	25	139.72	124.31	0.06
187	36	25	143.18	128.02	0.06
175	45	25	141.45	115.18	0.12
175	56	25	147.80	111.99	0.20
186	66	25	159.93	118.32	0.25
200	77	25	174.36	127.09	0.29
194	79	25	172.05	122.07	0.32
196	85	25	176.67	122.69	0.35
201	96	25	185.91	125.22	0.41
194	100	25	184.17	119.75	0.46
186	114	25	187.64	114.06	0.58
197	124	25	199.76	122.08	0.61
183	133	25	196.88	114.20	0.73
228	50	50	189.37	145.34	0.00
239	50	50	195.72	154.32	0.00
245	50	50	199.19	159.22	0.00
257	69	50	217.08	161.82	0.08
261	90	50	231.52	158.50	0.18
266	100	50	240.18	159.91	0.22
260	110	50	242.49	152.97	0.28
260	122	50	249.42	150.92	0.34
285	129	50	267.89	169.12	0.34
266	148	50	267.89	152.95	0.47
256	159	50	268.47	145.75	0.56

Table 5
Polyaxial test data for Solnhofen limestone [4].

σ_1 (MPa)	σ_2 (MPa)	σ_3 (MPa)	ξ (MPa)	ρ (MPa)	θ (rad)
397	20	20	252.30	307.82	0.00
417	51	20	281.75	312.26	0.07
413	92	20	303.11	295.90	0.17
453	165	20	368.35	311.69	0.34
460	206	20	396.06	312.36	0.43
465	233	20	414.54	314.76	0.50
449	40	40	305.42	333.95	0.00
446	40	40	303.69	331.50	0.00
486	80	40	349.87	348.98	0.08
499	113	40	376.43	348.81	0.15
530	193	40	440.52	354.53	0.31
547	274	40	497.10	358.86	0.48
535	315	40	513.84	350.74	0.59
473	60	60	342.37	337.21	0.00
517	87	60	383.36	362.62	0.05
537	102	60	403.57	373.51	0.08
530	113	60	405.88	364.05	0.10
576	164	60	461.88	385.93	0.19
550	197	60	465.92	357.53	0.27
553	275	60	512.69	349.55	0.45
557	345	60	555.41	352.69	0.61
528	80	80	397.22	365.79	0.00
572	126	80	449.18	384.32	0.08
577	150	80	465.92	380.45	0.13
647	208	80	539.82	420.55	0.22
591	225	80	517.31	372.43	0.28
677	283	80	600.44	429.28	0.34
665	298	80	602.18	418.11	0.38
650	378	80	639.70	403.19	0.55
680	454	80	700.90	428.54	0.67

Tables 9 and 10, respectively. In Table 9, the values in parenthesis are the best-fit parameters for M–C and H–B criteria taken from Colmenares and Zoback [14]. In the latter reference, the authors conducted a comparative study to examine different failure criteria for five rock types, viz. Shirahama sandstone, Yuubari shale, Dunham dolomite, Solnhofen limestone and KTB amphibolites, which are also among the eight rock types considered in this study. The parameters from Colmenares and Zoback were determined by the grid search method. It can be seen that, in general, the strength parameters from the grid search method are larger than those from the non-linear regression. For example, σ_c=250 MPa for KTB amphibolites, as estimated for H–B criterion by the grid search method, overestimates the actual test value, which is within the range 158 MPa $\leq \sigma_c \leq$ 176 MPa [1]. At the same time, σ_c,s determined by non-linear regression for HB and HB–WW criteria are 168 MPa and 175 MPa, respectively, which falls within the actual range. The values of ϕ and σ_c obtained from MC–JP criterion are consistently lower than those corresponding to M–C, except for Solnfhofen limestone, Mizuho trachyte and Manazuru andesite, for which σ_c from MC–JP criterion is slightly larger. The parameter m for both H–B and HB–WW criterion is within the range of typical values corresponding different rock types given in the literature [26]. It is evident that σ_c for H–B and HB–WW criterion is much lower than that for M–C and MC–JP, which is because of the non-linear form of H–B criterion.

The accuracy of the assessment of strength parameters based on the non-linear regression is clearly demonstrated by comparing the *RSD* values for M–C and H–B criteria with the corresponding values given in parenthesis in Table 10. The latter were calculated by employing the best fit parameters reported by Colmenares and Zoback [14]. For all five rock types, the misfit

Table 6
Polyaxial test data for Mizuho trahchyte [4].

σ_1 (MPa)	σ_2 (MPa)	σ_3 (MPa)	ξ (MPa)	ρ (MPa)	θ (rad)
302	45	45	226.32	209.84	0.00
314	58	45	240.76	214.53	0.04
327	67	45	253.46	221.82	0.07
341	90	45	274.82	225.57	0.14
350	138	45	307.73	221.07	0.30
359	204	45	351.03	222.04	0.53
368	281	45	400.68	236.36	0.78
353	323	45	416.27	240.17	0.96
341	60	60	266.16	229.44	0.00
353	83	60	286.37	230.42	0.07
386	133	60	334.29	241.95	0.22
401	186	60	373.55	243.85	0.37
403	212	60	389.71	243.06	0.46
401	254	60	412.81	241.89	0.60
381	306	60	431.28	237.47	0.82
368	75	75	299.07	239.23	0.00
405	108	75	339.48	257.03	0.09
415	147	75	367.77	253.38	0.20
438	210	75	417.42	259.47	0.38
440	279	75	458.42	258.69	0.59
430	318	75	475.16	256.66	0.73
452	363	75	513.84	278.68	0.82
437	100	100	367.77	275.16	0.00
463	126	100	397.79	286.36	0.06
493	171	100	441.10	296.18	0.17
497	256	100	492.48	282.86	0.40
522	354	100	563.49	300.46	0.64
510	384	100	573.89	297.00	0.74

Table 7
Polyaxial test data for Manazuru andesite [4].

σ_1 (MPa)	σ_2 (MPa)	σ_3 (MPa)	ξ (MPa)	ρ (MPa)	θ (rad)
364	20	20	233.25	280.87	0.00
381	20	20	243.06	294.76	0.00
470	67	20	321.58	349.82	0.10
516	124	20	381.05	369.91	0.20
538	186	20	429.55	374.07	0.32
552	40	40	364.89	418.05	0.00
577	75	40	399.53	424.89	0.06
632	112	40	452.64	456.82	0.11
669	126	40	482.09	482.32	0.13
653	206	40	519.04	448.38	0.26
626	278	40	545.02	416.79	0.42
671	70	70	468.23	490.71	0.00
735	101	70	523.08	530.77	0.04
735	152	70	552.52	512.78	0.11
808	193	70	618.34	559.17	0.16
812	275	70	667.99	541.90	0.27
801	313	70	683.58	526.48	0.33
833	375	70	737.85	543.13	0.41

(viz. *RSD* values) from the non-linear regression approach is much lower than from the grid search method, which implies that the strength parameters given in Colmenares and Zoback [14] are no longer the best fit values. This finding strongly suggests that the best fit parameters for MC–JP and HW–WW criteria are also accurate.

For each rock type in Table 10, the lower the *RSD* value, the lower the degree of misfit and the underscored numeral is the lowest *RSD*. It should be mentioned here that the comparison of *RSD* values between different rock types could be of little importance because the strengths differ from each other. As it is seen from the table, the HB–WW criterion results in the lowest *RSD* values for all rock types except for Yuubari shale, Solnhofen limestone and Mizuho trachyte, for which the lowest *RSD* values correspond to MC–JP criterion. Even for these three rock types, however, the lowest values are almost identical to those of HW–WW: in Yuubari shale, for example, the value 3.3121 for HB–WW is very close to the lowest value of 3.2017. Therefore, it is quite obvious that of the four criteria the HW–WW criterion fits the poly-axial test data best. Furthermore, it is apparent from the table that MC–JP criterion reproduces the experimental data better than M–C and H–B. Thus, we can conclude that the significant improvement in predicting the poly-axial strength could be achieved by selecting the proposed 3D rock failure criteria over the commonly used 2D criteria, which ignore the effect of the intermediate principal stress.

Table 8
Polyaxial test data for KTB Amphibolite [1,14].

σ_1 (MPa)	σ_2 (MPa)	σ_3 (MPa)	ξ (MPa)	ρ (MPa)	θ (rad)
165[a]	0	0	95.26	134.72	0.00
346	79	0	245.37	256.42	0.22
291	149	0	254.03	205.79	0.54
347	197	0	314.08	246.12	0.60
267	229	0	286.37	204.27	0.92
410	30	30	271.35	310.27	0.00
479	60	30	328.51	354.99	0.06
599	100	30	420.89	438.81	0.11
652	200	30	509.22	454.64	0.27
571	249	30	490.75	384.85	0.41
637	298	30	557.14	430.19	0.46
702	60	60	474.58	524.19	0.00
750	88	60	518.46	552.31	0.04
766	103	60	536.36	559.72	0.05
745	155	60	554.26	524.83	0.13
816	199	60	620.65	569.08	0.17
888	249	60	691.09	613.63	0.22
828	299	60	685.31	555.81	0.31
887	347	60	747.09	593.83	0.35
954	399	60	815.80	638.27	0.38
815	449	60	764.41	533.95	0.54
868	100	100	616.61	627.07	0.00
959	164	100	706.10	676.76	0.07
1001	199	100	750.56	698.76	0.10
945	248	100	746.51	638.16	0.16
892	269	100	728.04	589.90	0.20
1048	300	100	836.00	706.68	0.20
1058	349	100	870.07	702.96	0.25
1155	442	100	979.76	761.22	0.32
1118	597	100	1047.89	719.90	0.51
1147	150	150	835.43	814.05	0.00
1065	198	150	815.80	728.29	0.05
1112	199	150	843.51	766.25	0.05
1176	249	150	909.33	800.38	0.09
1431	298	150	1084.84	991.05	0.11
1326	348	150	1053.09	890.44	0.16
1169	399	150	991.89	751.28	0.24
1284	448	150	1086.57	831.40	0.26
1265	498	150	1104.47	806.77	0.31
1262	642	150	1185.88	788.04	0.46

[a] average value of three confined compressive strengths.

In Figs. 10 and 11, the strength predictions for eight different rocks, based on MC–JP and HB–WW criterion, are compared with the actual poly-axial test data in the $\sigma_1-\sigma_2$ plane. In these figures, the symbols represent the actual experimental data, while the solid curves are the corresponding predictions. Here, σ_1 values at failure for the same σ_3 are indicated with the same symbol. Both figures clearly show that the effect of the intermediate principal stress on the poly-axial strength is substantial. Also, it is evident that both 3D failure criteria proposed here fit the experimental test data quite well. In particular, the predictions for Shirahama sandstone, Yuubari shale and Mizuho trachyte are very accurate. Comparing the two criteria, HB–WW performs better than MC–JP criterion for lower values ofσ_3. This is clearly evident for the case of Shirahama sandstone, Westerly granite and KTB amphibolites, which is primarily because the strength of these rocks is highly non-linear with respect to the confining pressure.

Table 9
Best-fitting parameters from the non-linear multiple regression.

Rock type	M–C		MC–JP		H–B		HB–WW	
	$\phi(^\circ)$	σ_c (MPa)	$\phi(^\circ)$	σ_c (MPa)	m	σ_c (MPa)	m	σ_c (MPa)
Shirahama sandstone	39.43 (38.66)[a]	85 (95)	36.86	78	19.10 (18.20)	58 (65)	15.06	54
Yuubari shale	30.67 (26.57)	104 (120)	28.58	97	10.53 (6.50)	72 (100)	8.78	67
Westerly granite	52.00	328	50.27	295	36.77	260	33.30	230
Dunham dolomite	36.55 (33.02)	387 (450)	32.00	381	11.58 (8.00)	321 (400)	7.06	336
Solnhofen limestone	35.11 (28.81)	326 (375)	28.85	330	8.51 (4.60)	299 (370)	4.71	313
Mizuho trachyte	30.36	188	25.79	196	11.11	124	5.76	159
Manazuru andesite	49.40	284	44.80	297	46.49	150	19.36	236
KTB amphibolite	47.09 (50.19)	324 (300)	44.56	301	46.50 (30.00)	168 (250)	33.28	175

[a] The values in the parenthesis are the best-fitting parameters taken from Colmenares and Zoback [14].

Table 10
Residual standard deviation (*RSD*) of ρ at failure for eight rock types.

Rock type	M–C (MPa)	MC–JP (MPa)	H–B (MPa)	HB–WW (MPa)
Shirahama sandstone	4.4393 (4.9827)[b]	3.2374	4.1426 (4.7538)	2.4692[a]
Yuubari shale	5.8635 (6.4305)	3.2017	5.8676 (6.2326)	3.3121
Westerly granite	14.5147	11.3312	12.0914	6.8905
Dunham dolomite	22.0962 (24.2552)	12.2166	22.0541 (23.2993)	10.2227
Solnhofen limestone	16.2333 (18.0105)	8.8176	16.7120 (18.7368)	9.1346
Mizuho trachyte	11.3252	5.2440	11.3036	5.8529
Manazuru andesite	15.4644	9.2309	14.6840	7.0427
KTB amphibolite	27.2944 (33.4990)	22.0030	25.8111 (26.0379)	20.0405

[a] Underscored value is minimum *RSD* for the respective rock types.
[b] The values in the parenthesis are the RSD values when the best fit parameters in Colmenares and Zoback [14] are selected.

For Shirahama sandstone and Yuubari shale, the results corresponding to Modified Wiebols and Cook criterion [8], which is one of the well-known 3D rock failure criteria, are taken from Colmenares and Zoback [14] and reproduced in Fig. 12. These predictions are then compared with the ones corresponding to MC–JP and HB–WW criteria, viz. Figs. 10 and 11(a)–(b). Among the seven different failure criteria considered in their study, Colmenares and Zoback recommended the use of Modified Wiebols and Cook criterion for the prediction of poly-axial strength of rock. From the comparison, however, it is evident that the degree of misfit for Modified Wiebols and Cook is much higher than that for MC–JP and HB–WW criterion, which indicates that the proposed 3D failure criteria are quite adequate.

Another way of demonstrating the validity of the proposed 3D failure criteria is to plot the results of true triaxial tests in the deviatoric plane, as shown by Lade [27] for soil. For the deviatoric representation, a set of data satisfying the condition $\sigma_1+\sigma_2+\sigma_3=const.$ should be provided. As far as the authors know, there are no such true triaxial tests results for rocks available in the literature. For MC–JP criterion, however, given that the failure function is linear and the shape of deviatoric section is independent of ξ, i.e., the hydrostatic stress, the plot of the octahedral section is possible if all the data points are projected on the deviatoric plane whose distance from the apex of the failure surface is 1. This projection is equivalent to the normalization of ρ by $(\xi+\sqrt{3}c\cot\phi)$. In Fig. 13, the true triaxial test data are plotted in the projected deviatoric plane, together with the best-fit approximations based on MC–JP criterion, for four rock types, i.e., Shirahama sandstone, Yuubari shale, Mizuho trachyte, and KTB amphibolites,. With the assumption that the rock samples are isotropic, the test data are projected in all six sectors of the octahedral section. This figure clearly shows that MC–JP criterion gives an accurate representation of the conditions at failure in the deviatoric plane. It is also noted that the experimental data are positioned along the best-fitting convex curve, which strongly confirms the effect of the intermediate principal stress on the rock strength.

6. Extension to anisotropic conditions

As pointed out by Lee and Pietruszczak [28], the σ_2-dependence of rock strength could be partly attributed to inherent anisotropy of the rock material, which is closely related to the microstructure, such as grain arrangement, foliation, bedding, joint pattern, etc. The proposed 3D criteria, viz. MC–JP and HB–WW, can be extended to their respective anisotropic versions by postulating that the strength parameters depend on the orientation of the sample relative to the loading direction. Such an approach, which provides a simple generalization of isotropic frameworks, requires an appropriate evolution laws for the related strength parameters.

In order to illustrate the methodology, both H–B and HB–WW criteria are extended to anisotropic conditions based on the microstructure tensor approach proposed by Pietruszczak and Mroz [29]. Restricting the considerations to compressive regime, it is assumed that uniaxial strength σ_c is orientation-dependent, while m is kept constant. According to the microstructure tensor approach, the spatial variation of σ_c can be described by introducing a scalar-valued function

$$\sigma_c=\sigma_{c0}[1+A_{ij}l_il_j+b_1(A_{ij}l_il_j)^2+b_2(A_{ij}l_il_j)^3+b_3(A_{ij}l_il_j)^4+\cdots] \tag{24}$$

Here, A_{ij} is a traceless symmetric tensor representing the bias in the distribution of σ_c. Its eigenvectors coincide with the principal material triad $\boldsymbol{e}^{(i)}(i=1,2,3)$. Apparently, for an isotropic material there is $A_{ij}=0$ so that $\sigma_c=const.$ The expansion coefficients b_1, b_2,... as well as σ_{c0} are constants, whereas l_i specifies the generalized loading direction. The latter is defined as

$$l_i=\frac{T_i}{\sqrt{L_kL_k}};\quad L_i=T_ke_i^{(k)} \tag{25}$$

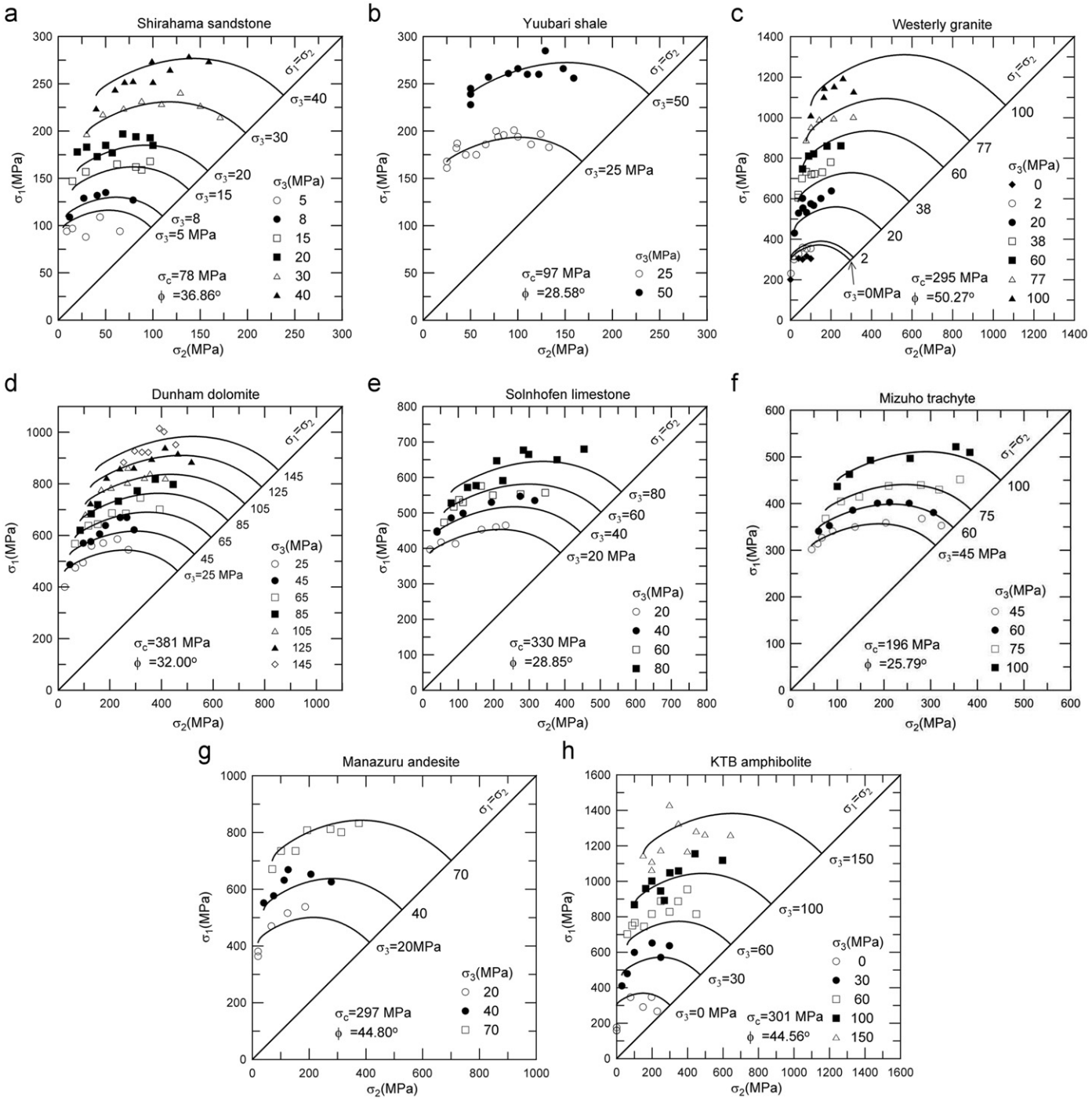

Fig. 10. Best-fitting the polyaxial test data with the MC–JP criterion; (a) Shirahama sandstone, (b) Yuubari shale, (c) Westerly granite, (d) Dunham dolomite, (e) Solnhofen limestone, (f) Mizuho trachyte, (g) Manazuru andesite, (h) KTB amphibolites.

where L_i is referred to as the loading vector and $T_i = \|\sigma_{jk} e_k^{(i)}\|$ are the traction moduli on the plane normal to the principal triad $\boldsymbol{e}^{(i)}$. According to Eqs. (24) and (25), the value of σ_c is a function of mixed invariants of the stress and the microstructure tensor A_{ij}.

Fig. 14 shows an example of parameters' identification taken from Pietruszczak et al. [30], where the authors fitted the spatial variation of uniaxial strength of Tournemire shale by incorporating the terms up to order 4. The shale is a transversely isotropic rock so that for the uniaxial loading process ($\sigma_2 = \sigma_3 = 0$), considering the traceless nature of A_{ij}, the term $A_{ij} l_i l_j$ simplifies to $A_1(1 - 3\cos^2 d)$. In this case, the following coefficients were obtained from the best fit curve shown in Fig. 14,

$$\sigma_{c0} = 22 \text{ MPa}; \quad A_1 = 0.0170251;$$
$$b_1 = 515.49; \quad b_2 = 61735.3; \quad b_3 = 2139820.0 \tag{26}$$

Using now the spatial distribution function Eq. (24) and employing the parameters given in Eq. (26), a series of numerical simulations of poly-axial tests was carried out to demonstrate the difference in strength predictions between isotropic H–B and HB–WW criteria and their respective anisotropic versions. Fig. 15 shows the loading configuration along with the corresponding strength predictions. In the analysis, the minimum principal

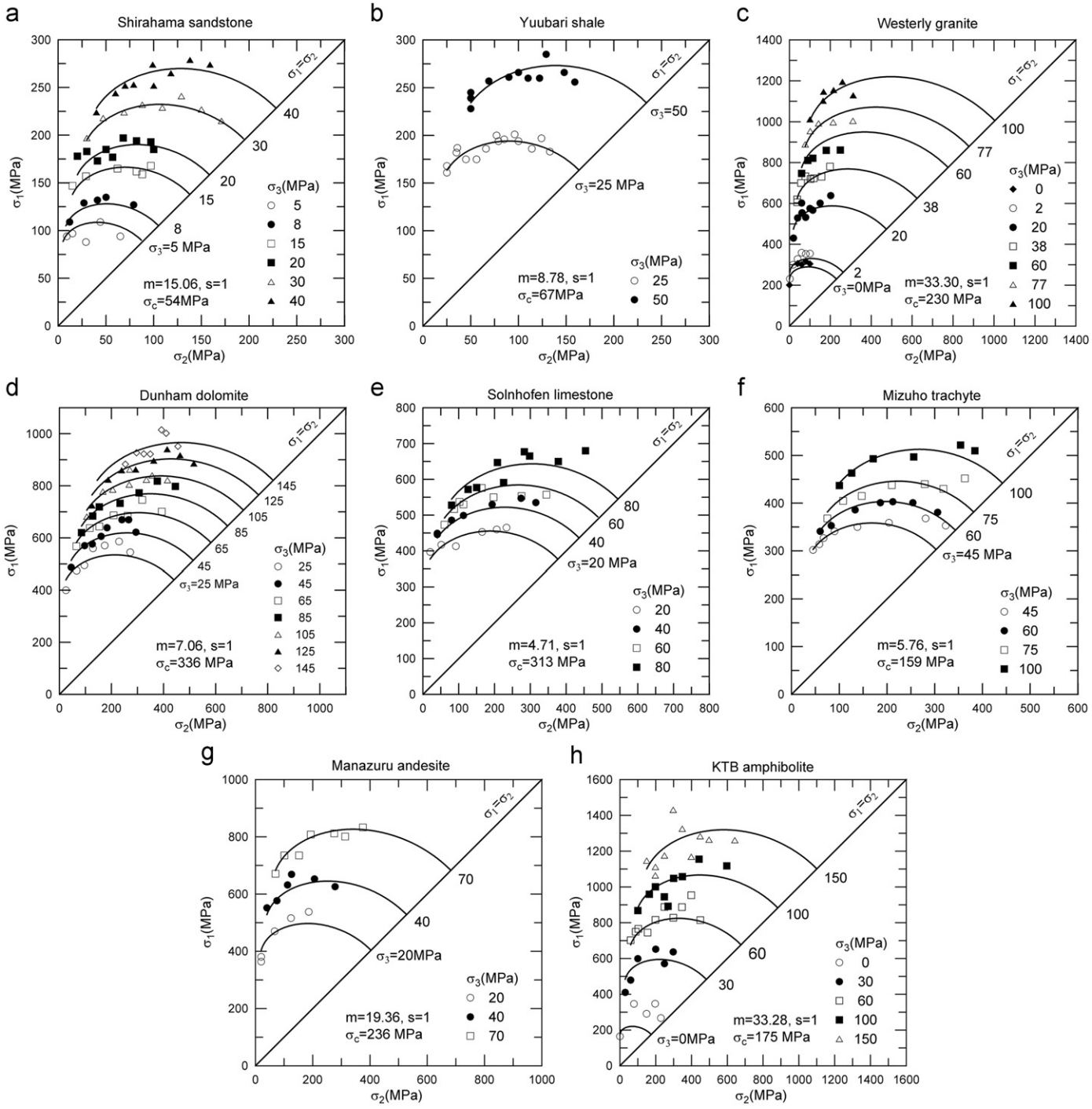

Fig. 11. Best-fitting the polyaxial test data with the HB–WW criterion; (a) Shirahama sandstone, (b) Yuubari shale, (c) Westerly granite, (d) Dunham dolomite, (e) Solnhofen limestone, (f) Mizuho trachyte, (g) Manazuru andesite, (h) KTB amphibolites.

stress of $\sigma_3=10$ MPa was applied along the direction of x_1-axis. The dip angle (d) of weakness planes was 60° and was kept constant, while four cases of dip direction (φ), viz. $\varphi=0°$, 30°,45°,90°, were considered in the analysis. Note that $\varphi=0°$ means that the strike of weakness plane is parallel to the direction of σ_2, whereas for $\varphi=90°$ it is perpendicular to the direction of σ_2. The calculations were carried out for $m=6.0$, which is a typical value for shale [26], and $s=1.0$. In addition, for the isotropic criteria, the value of $\sigma_c=22$ MPa was assumed, which corresponds to $A_{ij}=0$ in Eq. (24).

Based on results in Fig. 15, it is evident that the strength of Tournemire shale depends on the orientation of weakness planes with respect to given stress conditions. For the considered loading configuration, the strengthening effect of σ_2 is more pronounced as the strike of weakness planes gets closer to the direction of σ_2. It is interesting to note that the H–B criterion, which ignores the effect of σ_2 for isotropic rock, predicts an increase in strength with σ_2 for $\varphi<45°$, whereas the strength is slightly reduced with σ_2 for $\varphi>45°$. The result indicate that, for the criteria considered here, the influence of σ_2 on the strength of transversely isotropic rock is minimized if the strike of weakness plane approaches the direction of the minor principal stress σ_3. Once again, the results confirm that the anisotropic versions of H–B and HB–WW criteria predict the same strength for the case of triaxial compression

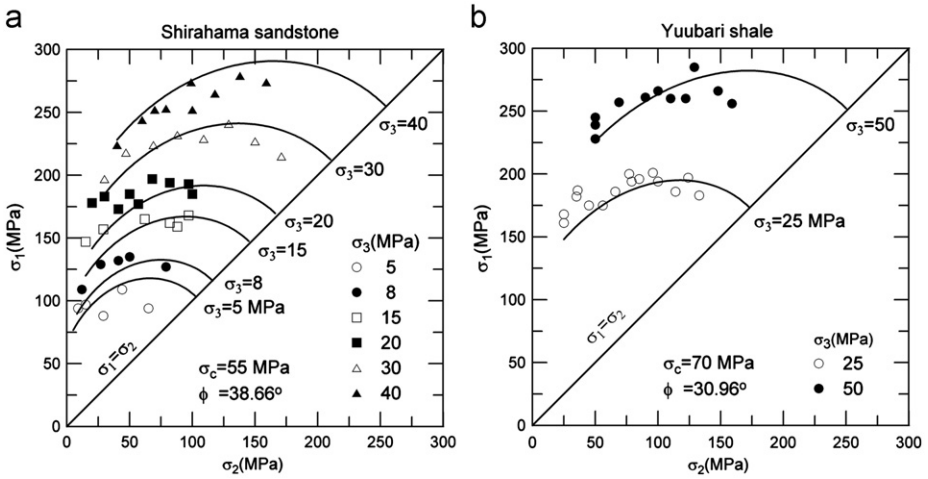

Fig. 12. Fitting the polyaxial test data with the Modified Wiebols and Cook criterion using Colmenares and Zobak's best-fitting parameters; (a) Shirahama sandstone, (b) Yuubari shale.

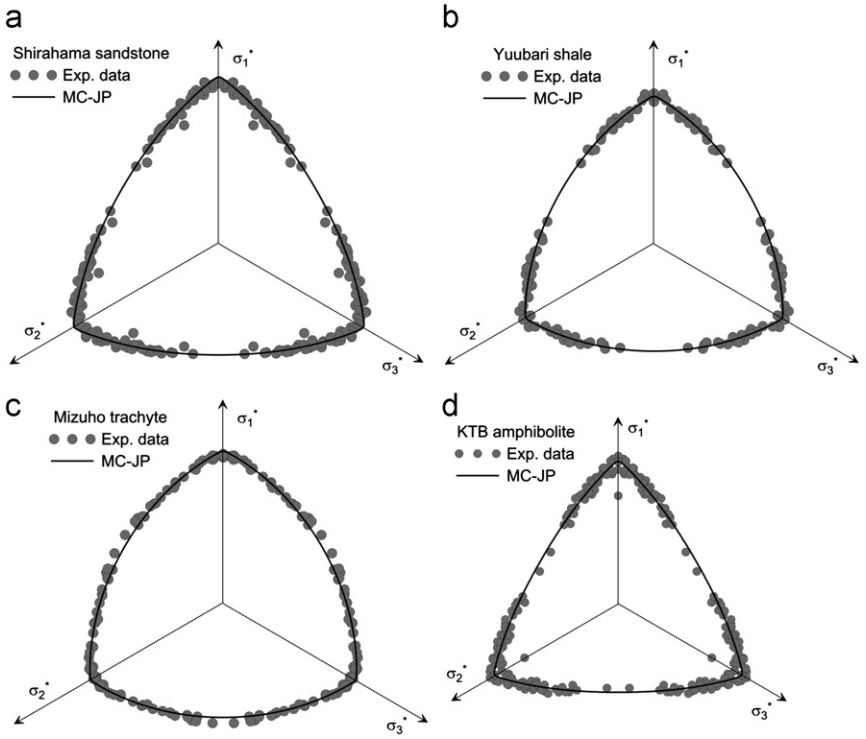

Fig. 13. The polyaxial test data in the projected deviatoric plane along with the best-fitting section of MC–JP criterion; (a) Shirahama sandstone, (b) Yuubari shale, (c) Mizuho trachyte, (d) KTB amphibolites.

($\sigma_1 > \sigma_2 = \sigma_3$) and extension ($\sigma_1 = \sigma_2 > \sigma_3$), which is due to the fact that two criteria still coincide along the corners of respective failure surfaces. Based on the discussion and the results given above, it may be concluded that the effect of σ_2 on the strength of rock could be partly attributed to the specific features of the material microstructure.

7. Conclusions

Despite several shortcomings, M–C and H–B criteria have been widely accepted in the rock mechanics community, which is mainly due to their simplicity and the large amount of experimental data available for their identification. Both these criteria ignore the strengthening effect of the intermediate principal stress. In addition, they pose mathematical difficulties as their gradients are not uniquely defined along the meridian loci corresponding to triaxial compression and extension regimes. In order to overcome these limitations, a significant research effort has been devoted to modify the functional form of these criteria; this has also been the main goal of the study pursued here.

The proposed 3D versions of M–C and H–B criteria, referred to as MC–JP and HB–WW, respectively, have been formulated in terms of Nayak and Zienkiewicz's stress invariants, viz. ξ, ρ, and θ, to facilitate the selection of the best fit strength parameters from the poly-axial test data. The proposed criteria have the same meridian sections as the original ones, in both the triaxial compression and the extension regimes, whereas the deviatoric sections are modified to accommodate the requirements of both convexity and smoothness. The modifications for MC–JP and HB–

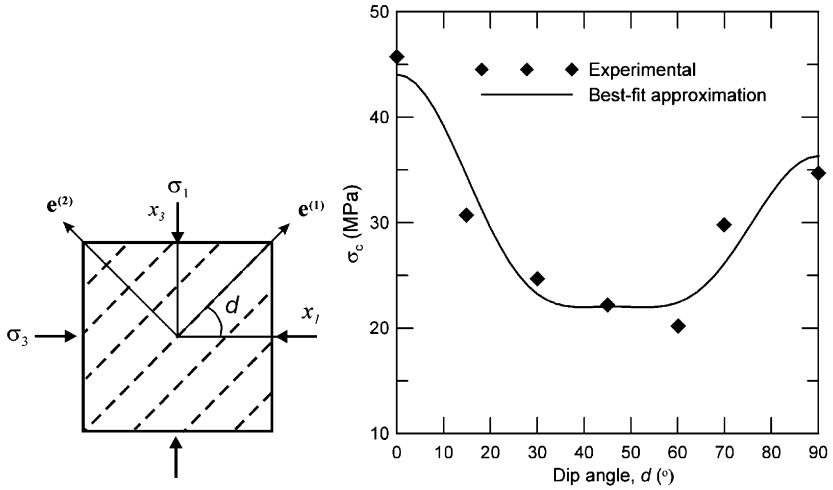

Fig. 14. Variation of $\sigma_c$with sample orientation, d, in Tournemire shale [30].

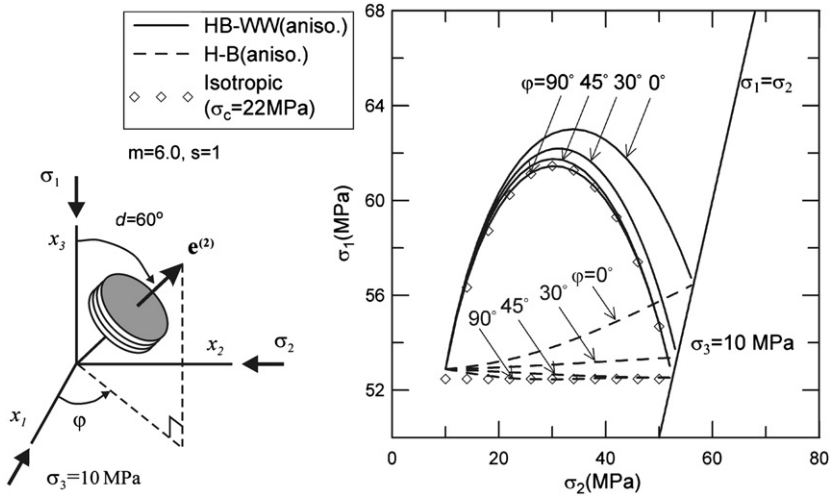

Fig. 15. Effect of σ_2 on the rock strength with the consideration of transversely anisotropy in σ_c.

WW criteria have been accomplished by adopting the deviatoric shape functions proposed by Jiang and Pietruszczak [22] and Willam and Warnke [23], respectively. The proposed criteria inherit all key characteristics of the original ones and incorporate the same strength parameters, which is an encouraging feature for the potential use in engineering practice. Moreover, the proposed failure surfaces are smooth and convex for a wide range of strength parameters.

The accuracy of MC–JP and HB–WW criteria has been validated for eight rock types whose poly-axial test data are available in the literature. The best-fitting parameters for each failure criterion were determined through a non-linear multiple regression analysis on the whole poly-axial test data simultaneously, which resulted in a very accurate estimation of the strength parameters. Comparison of the strength predictions of MC–JP and HB–WW criteria with the actual experimental data shows that the overall performance of both these criteria is excellent. For low confining pressures, HB–WW criterion gives better predictions than MC–JP. Furthermore, the result of the non-linear regression analysis reveal that the grid search method for selecting the best fit parameters from poly-axial test data is not accurate.

An extension of the proposed failure criteria to the case of inherent anisotropy has been discussed to broaden the range of application. Using the assumption of transverse isotropy, H–B and HB–WW criteria have been extended to their corresponding anisotropic forms based on the microstructure tensor approach. The results of an illustrative example provided suggest that the alignment of structural defects may result in a more pronounced σ_2 dependency of strength.

Finally, it should be mentioned that studies on the application of the proposed failure criteria to the analysis of some practical engineering problem are under way and the results will be reported in near future.

Acknowledgements

This research was supported by Basic Science Research Program through the National Research Foundation of Korea (NRF) funded by the Ministry of Education, Science and Technology (No.2011-0014012).

References

[1] Chang C, Haimson B. True triaxial strength and deformability of the German Continental Deep Drilling Program (KTB) deep hole amphibolites. J Geophys Res 2000;105:18999–9013.
[2] Haimson B, Chang C. A new true triaxial cell for testing mechanical properties of rock, and its use to determine rock strength and deformability of Westerly granite. Int J Rock Mech Min Sci 2000;37:285–96.

[3] Hoskins ER. The failure of thick-walled hollow cylinders of isotropic rock. Int J Rock Mech Min Sci 1969;6:99–125.
[4] Mogi K. Experimental rock mechanics. London: Taylor & Francis; 2007.
[5] Takahashi M, Koide H. Effect of the intermediate principal stress on strength and deformation behavior of sedimentary rocks at the depth shallower than 2000 m. In: Maury V, Fourmaintraux D, editors. Rock at great depth, 1. Rotterdam: Balkema; 1989. p. 19–26.
[6] Drucker D, Prager W. Soil mechanics and plastic analysis or limit design. Q Appl Math 1952;10:157–65.
[7] Ewy R. Wellbore stability predictions by use of a modified Lade criterion. SPE Drill Completion 1999;14(2):85–91.
[8] Zhou S. A program to model the initial shape and extent of borehole breakout. Comput Geosci 1994;20:1143–60.
[9] Al-Ajmi AM, Zimmerman RW. Relation between the Mogi and the Coulomb failure criteria. Int J Rock Mech Min Sci 2005;42:431–9.
[10] Zhang L, Zhu H. Three-dimensional Hoek–Brown strength criterion for rock. J Geotech Geoenviron Eng 2007;133:1128–35.
[11] Benz T, Schwab R, Kauther RA, Vermeer PAA. Hoek–Brown criterion with intrinsic material strength factorization. Int J Rock Mech Min Sci 2008;45:210–22.
[12] Yu MH, Zan YW, Zhao J, Yoshimine M. A unified strength criterion for rock material. Int J Rock Mech Min Sci 2002;39:975–89.
[13] Benz T, Schwab R. A quantitative comparison of six rock failure criteria. Int J Rock Mech Min Sci 2008;45:1176–86.
[14] Colmenares LB, Zoback MD. A statistical evaluation of intact rock failure criteria constrained by polyaxial test data for five different rocks. Int J Rock Mech Min Sci 2002;39:695–729.
[15] Priest SD. Comparison between selected three-dimensional yield criteria applied to rock. Rock Mech Rock Eng 2010;43:379–89.
[16] Al-Ajmi AM, Zimmerman RW. Stability analysis of vertical boreholes using the Mogi–Coulomb failure criterion. Int J Rock Mech Min Sci 2006;43:1200–11.
[17] Zhang L, Cao P, Radha KC. Evaluation of rock strength criteria for wellbore stability analysis. Int J Rock Mech Min Sci 2010;47:1304–16.
[18] Zhou XP, Yang HQ, Zhang YX, Yu MH. The effect of the intermediate principal stress on the ultimate bearing capacity of a foundation on rock masses. Comput Geotech 2009;36:861–70.
[19] Morris AP, Ferrill DA. The importance of the effective intermediate principal stress (σ'_2) to fault slip patterns. J Struct Geol 2009;31:950–9.
[20] Nayak GC, Zienkiewicz OC. Convenient forms of stress invariants for plasticity. J Struct Div ASCE 1972;98:949–53.
[21] Drucker DC. A definition of stable inelastic material. J Appl Mech 1959;26:101–6.
[22] Jiang J, Pietruszczak S. Convexity of yield loci for pressure sensitive materials. Comput Geotech 1988;5:51–63.
[23] Willam KJ, Warnke EP. Constitutive model for triaxial behavior of concrete. Colloquium on concrete structures Subjected to triaxial stresses. ISMES Bergamo, IABSE Report 1972:19.
[24] Hoek E, Brown ET. Underground excavations in rock. London: Institution Min & Metall; 1980.
[25] Davis JC. Statistics and data analysis in geology. 3rd ed. London: Wiley; 2002.
[26] Brady BHG, Brown ET. Rock mechanics for underground mining. 3rd ed. Dordrecht: Kluwer; 2004.
[27] Lade PV. Modelling the strength of engineering materials in three dimensions. Mech Cohes Frict Mater 1997;2:339–56.
[28] Lee YK, Pietruszczak S. Application of critical plane approach to the prediction of strength anisotropy in transversely isotropic rock masses. Int J Rock Mech Min Sci 2008;45:513–23.
[29] Pietruszczak S, Mroz Z. Formulation of anisotropic failure criteria incorporating a microstructure tensor. Comput Geotech 2000;26:105–12.
[30] Pietruszczak S, Lydzba D, Shao JF. Modelling of inherent anisotropy in sedimentary rocks. Int J Solids Struct 2002;39:637–48.